# A linear benchmark between HYMAGYC, MEGA and ORB5 codes using the NLED-AUG test case to study Alfvénic modes driven by energetic particles

**G. Vlad[1], X. Wang[2], F. Vannini[2], S. Briguglio[1], N. Carlevaro[1], M. Falessi[1], G. Fogaccia[1], V. Fusco[1], F. Zonca[1,3], A. Biancalani[2], A. Bottino[2], T. Hayward-Schneider[2], Ph. Lauber[2]**

[1]ENEA, FSN, C. R. Frascati, Via E. Fermi 45, 00044 Frascati (Roma), Italy
[2]Max-Planck-Institut für Plasmaphysik, Boltzmannstr. 2, 85748 Garching, Germany
[3]Institute for Fusion Theory and Simulation and Department of Physics, Zhejiang University, Hangzhou 310027, People's Republic of China

E-mail: gregorio.vlad@enea.it

**Abstract.** One of the major challenges in magnetic confinement thermonuclear fusion research concerns the confinement of the energetic particles (EPs) produced by fusion reactions and/or by additional heating systems. In such experiments, EPs can resonantly interact with the shear Alfvén waves. In the frame of the EUROfusion 2019-2020 Enabling Research project "Multi-scale Energetic particle Transport in fusion devices" (MET), a detailed benchmark activity has been undertaken among few of the state-of-the-art codes available to study the self-consistent interaction of an EP population with the shear Alfvén waves. In this paper linear studies of EP driven modes with toroidal mode number $n = 1$ will be presented, in real magnetic equilibria and in regimes of interest for the forthcoming generation devices (e.g., ITER, JT-60SA, DTT). The codes considered are HYMAGYC, MEGA, and ORB5, the first two being hybrid MHD-Gyrokinetic codes (bulk plasma is represented by MHD equations, while the EP species is treated using the gyrokinetic formalism), the third being a global electromagnetic gyrokinetic code. The so-called NLED-AUG reference case has been considered, both for the peaked on-axis and peaked off-axis EP density profile cases, using its shaped cross section version. Comparison of the spatial mode structure, growth rate and real frequency of the modes observed will be considered in detail. The dependence of mode characteristics when several parameters are varied, as, e.g., the ratio between EP and bulk ion density and energetic particle temperature, will be presented. A remarkable agreement is observed among the three codes for the peaked off-axis case, obtaining all of them a TAE localized close to the magnetic axis. On the other hand, some differences are observed when considering the peaked on-axis case, where two modes are observed (a TAE localized in the radial external region, and a RSAE around mid-radius). A careful analysis of the stability of this equilibrium, in particular by varying self-consistently the EP drive, will allow to reconcile the results of the three codes.

*Keywords*: hybrid MHD-gyrokinetic simulation, gyrokinetic simulation, energetic particles, Alfvénic modes, numerical simulations, particle-in-cell method, ideal and resistive MHD modes

Submitted to: *Nuclear Fusion*

## 1. Introduction

One of the major challenges in magnetic confinement thermonuclear fusion research concerns the confinement, inside the reaction chamber, of the Energetic Particles (EPs) produced by fusion reactions and/or by additional heating systems, as, e.g., electron and ion cyclotron resonant heating, and neutral beam injection. In such experiments, EPs, having their velocities of the order of the Alfvén velocity, can resonantly interact with the shear Alfvén waves. In order to predict and, eventually, minimize the EP transport in the next generation fusion devices, several numerical models, based on different theoretical approaches, have been developed. In this respect, it is crucial to cross verify and validate the different numerical instruments available in the fusion community. For this purpose, in the frame of the EUROfusion 2019-2020 Enabling Research project "Multi-scale Energetic particle Transport in fusion devices" (MET) [1], a detailed benchmark activity has been undertaken among few of the state-of-the-art codes available to study the self-consistent interaction of an EP population with the shear Alfvén waves, in real magnetic equilibria and in regimes of interest for the forthcoming generation devices (e.g., ITER [2], JT-60SA [3], DTT [4]). The codes considered in this benchmark are HYMAGYC [5, 6, 7], MEGA [8, 9, 10], and ORB5 [11, 12, 13], the first two being hybrid MHD-Gyrokinetic codes (bulk plasma is represented by MHD equations, while the EP species is treated using the gyrokinetic formalism), the third being a global electromagnetic gyrokinetic code (both bulk and EP species are treated using the gyrokinetic formalism). The so-called NLED-AUG [14] reference case has been considered, both for the peaked on-axis and peaked off-axis EP density profile cases, using its shaped cross section version. This test case poses an exceptional challenge to the codes due to its high EP pressure, the rich spectrum of experimentally observed instabilities and their non-linear interaction [15].

Particular care has been devoted to consider plasma and numerical parameters as close as possible among the three codes: the same input equilibrium file (EQDSK) has been considered, ion density profile has been obtained by imposing quasi-neutrality ($Z_i n_i + Z_h n_h = n_e$), as required by ORB5 (here $n_i, n_e, n_h$ are the bulk ions, electrons, and EP densities (both bulk ion and EPs are assumed to be Deuterons), respectively, and $Z_i, Z_h$ their electric charge numbers); finite resistivity and adiabatic index $\Gamma = 5/3$ have been assumed for both the hybrid codes (this is the usual choice used in MEGA, where also some viscosity is considered to help numerical convergence). Only finite orbit width (FOW) effects have been retained in this benchmark, and an isotropic Maxwellian EP distribution function of Deuterons with $T_h$=0.093 MeV, constant in radius, has been considered. Perturbations with single toroidal mode number $n = -1$ will be studied.

The paper is organized as follows: in Sec. 2 a brief description of the codes participating to this benchmark will be given, as well as the setting up of the benchmark equilibrium and the specific code parameters used; in Sec. 3 a characterization of the equilibrium in the MHD limit will be presented; in Sec. 4 the results of linear simulations will be presented: for the nominal cases in Subsec. 4.1, for the results of scanning the

EP density in Subsec. 4.2, as well as for the results of scanning the EP temperature in Subsec. 4.3; in Sec. 5 some concluding remarks will be drawn.

## 2. Codes, equilibrium and numerical parameters

As anticipated in the Introduction, Sec. 1, three codes has been considered for this benchmark: HYMAGYC, MEGA, and ORB5. The HYMAGYC code is a Hybrid Magnetohydrodynamics Gyrokinetic Code suitable to study EP driven Alfvénic modes in general high-$\beta$ axisymmetric equilibria, (with $\beta$ being the ratio of the plasma pressure to the magnetic pressure), with perturbed electromagnetic fields (electrostatic potential $\varphi$ and vector potential $\mathbf{A}$) fully accounted for. The thermal plasma is described by linear, full, resistive MHD equations in arbitrary axis-symmetric equilibria. The MHD field solver relies on equilibrium quantities computed by the high resolution equilibrium code CHEASE [16] (as, e.g., covariant and contravariant components of the metric tensor coefficients, Jacobian, equilibrium magnetic field, current density components and pressure); it is also fully interfaced with the European Integrated Modelling Framework data structure [17] (formerly ITM, presently maintained by the EU-IM Team‡) and the IMAS environment [18]. Such field solver originates from the full, linear, resistive MHD code MARS [19], which has been transformed from an eigenvalue solver to an initial value one (see Appendix A.2 in [20]) which uses a fully implicit (backward Euler) finite difference time discretization scheme. The MARS kernel uses Fourier decomposition in generalized poloidal ($\chi$) and toroidal ($\phi$) angles and generalized finite element method along with the Tunable Integration Method [21] for the discretization in the radial-like coordinate $s = \sqrt{|\psi - \psi_0|/|\psi_{edge} - \psi_0|}$ (with $\psi$ the equilibrium poloidal flux function, and $\psi_0$ and $\psi_{edge}$, respectively, the value of $\psi$ on the magnetic axis and on the last closed magnetic surface). The EP population is described by the nonlinear gyrokinetic Vlasov equation, solved by particle-in-cell (PIC) techniques, and expanded up to order $\mathrm{O}(\epsilon^2)$ and $\mathrm{O}(\epsilon\epsilon_B)$, $\epsilon$ being the gyrokinetic ordering parameter $\epsilon \sim \rho_h/L_n$ and $\epsilon_B \sim \rho_h/L_B$, with $\rho_h$ the energetic ("hot") particle Larmor radius, $L_n$ and $L_B$ the characteristic equilibrium plasma density and magnetic-field nonuniformity length scales, respectively. As $L_n/L_B \ll 1$, $\mathrm{O}(\epsilon_B^2)$ terms are neglected. The standard $\delta f$ method for the EP distribution function is used, i.e., the EP distribution function is written as $F_h = F_{h,0} + \delta f_h(t)$, with $F_{h,0}$ the initial, time-independent EP distribution function, and the Vlasov equation is solved for $\delta f_h(t)$. The perturbed electromagnetic fields are assumed to be low-frequency fluctuations characterized by short wavelengths perpendicular to the equilibrium magnetic field and long wavelengths parallel to it. The following space-time ordering for the fluctuating electromagnetic fields holds [22]: $k_\perp \rho_h = O(1)$, $k_\parallel \rho_h = O(\epsilon)$, $\omega/\Omega_h = O(\epsilon)$, being $k_\perp$ the perpendicular (to the equilibrium magnetic field) wave vector of perturbed fields, $k_\parallel$ the parallel one, $\omega$ the characteristic fluctuation frequency and $\Omega_h = q_h B/m_h c$ the EP gyrofrequency, with $q_h$, $m_h$, $B$ and $c$ the EP charge and mass, the equilibrium magnetic field and the light

‡ See `http://www.euro-fusionscipub.org/eu-im`

velocity, respectively. Flux coordinate system ($s$, $\chi$, $\phi$) is used. The MHD solver can consider finite resistivity $\eta$ and finite adiabatic index $\Gamma$, but no viscosity. Generation of fluctuation structures at small scale is not a concern for the present linear simulations, which are not affected by spectral cascade. However, it may be worthwhile informing the readers that generation of mean or zonal flows, and more generally zonal structures [23], plays a crucial role in determining the saturation level of Alfvénic as well as drift wave fluctuations. In this respect, collisionless dissipation of zonal structures must be properly reproduced, and the absence of viscosity in HYMAGYC is a crucial element for us to investigate the effect of fluctuation suppression by the residual flow§. The coupling between MHD and EPs is obtained by adding to the MHD momentum equation a term proportional to $\nabla \cdot \Pi_k$ [24] ($\Pi_k$ being the EP stress tensor). The field solver of HYMAGYC describes, within the full MHD, resistive model considered for describing the bulk plasma, both continuum damping and, eventually, resistive damping. The gyrokinetic module, on the other side, retains Landau damping for the EP species, besides the EP drive. Note that HYMAGYC can retain also kinetic effects for the bulk ion species by using an extended hybrid model [25], which would require to evolve, gyrokinetically, an additional particle population representing bulk ions, but this opportunity is not considered in this paper.

In the MEGA code [8, 9, 10], the bulk plasma is described using nonlinear full MHD equations, and the EPs are described by the drift-kinetic equation. The energetic ion contribution is included in the MHD momentum equation as the EP current density $j'_h$ that includes the contributions from parallel velocity, magnetic curvature and gradient drifts, and magnetization current. The $E \times B$ drift disappears in $j'_h$ owing to quasi-neutrality. The standard $\delta f$ method is used for evolving the EP distribution function. The electromagnetic field is given by the standard MHD description, or by the Hazeltine and Meiss equations [26]. The MHD equations are solved using a finite-difference scheme of fourth-order accuracy in space and time. Resistivity, viscosity and diffusion terms are included in the equations. Moreover, an adiabatic index $\Gamma = 5/3$ is also used in the MHD solver. Note that $(R, \phi, Z)$ coordinates are used for solving the equations, while flux coordinates are considered for the result analysis; note that a Fourier filter is used in the $\phi$ direction, in order to retain the toroidal components $n = -1, 0, +1$. In the present paper only standard MHD description will be considered. The various damping retained by MEGA are similar to the ones mentioned for HYMAGYC, besides the viscous damping which is included in MEGA.

ORB5 [11, 12, 13] is a global, nonlinear, electromagnetic, particle-in-cell code which solves the gyrokinetic Vlasov-Maxwell system of equations described in Refs. [27, 28]. It can take into accounts collisions and heat, particle and momentum sources (which are neglected in the present work). The distribution function of each species "$sp$" is composed by a time-independent background component $F_{0,sp}$ and a time-dependent part $\delta f_{sp}$. The latter is represented by sample of numerical particles (markers), which

§ these studies will be reported elsewhere.

are pushed with a 4th-order Runge-Kutta scheme along the trajectories defined by the equation of motion of the gyrocenter characteristics $(\vec{R}, v_\parallel, \mu)$. In ORB5 straight field-line coordinates are used: $(s, \theta^*, \phi)$. The radial coordinate, $s$, is the same used by the code HYMAGYC, and defined before. The angular coordinates are the torodial angle $\phi$ and the poloidal magnetic angle $\theta^* = q^{-1}(s) \int_0^\theta [(\vec{B} \cdot \nabla\phi)/(\vec{B} \cdot \nabla\theta')] d\theta'$, where $q(s)$ is the safety factor profile and $\theta$ the geometric poloidal angle. The equations of motion are coupled with the field equations: the Poisson equation (in the quasi-neutrality limit) and the parallel Ampère's law. These are solved using finite elements (typically cubic B-splines) on a grid $(N_s, N_{\theta^*}, N_\phi)$. A field-aligned Fourier filter is used [11]. At each radial grid point $s$, for each toroidal mode $n$, only the poloidal modes $m \in [-n \cdot q(s) \pm \Delta m]$ are retained, being $\Delta m$ the width of the retained poloidal modes. The equations are solved through a mixed-variable pullback algorithm in order to mitigate the so-called cancellation problem [29]. ORB5 considers a filter in the $\phi$ direction, and here only the modes with toroidal mode number $n = \pm 1$ are retained and initialized. By being fully gyrokinetic, ORB5 retains Landau damping for all the species considered, i.e., electrons, bulk ions and EPs; continuum damping is also retained [30]. It can be shown that the gyrokinetic model implemented in ORB5 contains the MHD equations as a subset [31]. The interested reader can find more details about this point in [32, 33].

For the purpose of this benchmark, all the codes will consider only Finite Orbit Width (FOW) effects when describing EPs, neglecting Finite Larmor radius (FLR) ones, as already stated in the Introduction, Sec. 1.

The equilibrium chosen for this benchmark is a "variant" of the AUG test case, originally proposed by Ph. Lauber within the EUROfusion Enabling Research NLED [14]: the AUG shot considered is the #31213, at t=0.84s. In order to use such test case to execute this benchmark on a realistic, fully shaped equilibrium, we have considered the fully shaped cross section version of this equilibrium [14], as described by a standard EQDSK file (see Fig. 1). The equilibrium, as defined in the original AUG EQDSK file, has been scaled using the equilibrium code CHEASE [16] in order to keep exactly the on-axis safety factor $q_0$ as tabulated in the EQDSK file itself, namely $q_0 \simeq 2.39897$: this choice results in a toroidal Alfvén gap fully open, when considering the reference bulk mass plasma density profile. Also, the experimental equilibrium has been transformed such to have both positive toroidal magnetic field and plasma current, when considering the coordinate system ($R$, $Z$, $\phi$) used by CHEASE [16], and ($s$, $\chi$, $\phi$) used by HYMAGYC (also described by the so-called COCOS number [34], COCOS=2). As a final remark, the plasma boundary has been slightly smoothed, in order to remove the sharpness of the experimental AUG X-point (both CHEASE and HYMAGYC assume closed magnetic surface domain). As a result of these approximations, a new EQDSK file has been shared among the different codes for the benchmark exercise, being characterized by on-axis toroidal magnetic field $B_0 \simeq 2.208$ [T], on-axis major radius $R_0 \simeq 1.666$ [m], plasma current $I_p \simeq 8.1434 \times 10^5$ [A], inverse aspect ratio $\epsilon_0 \simeq 0.297898$.

Electron and energetic particle (Deuterium) density profiles are shown in Fig. 2, as given by the original NLED-AUG case [14]: two variants for the EP density profile are

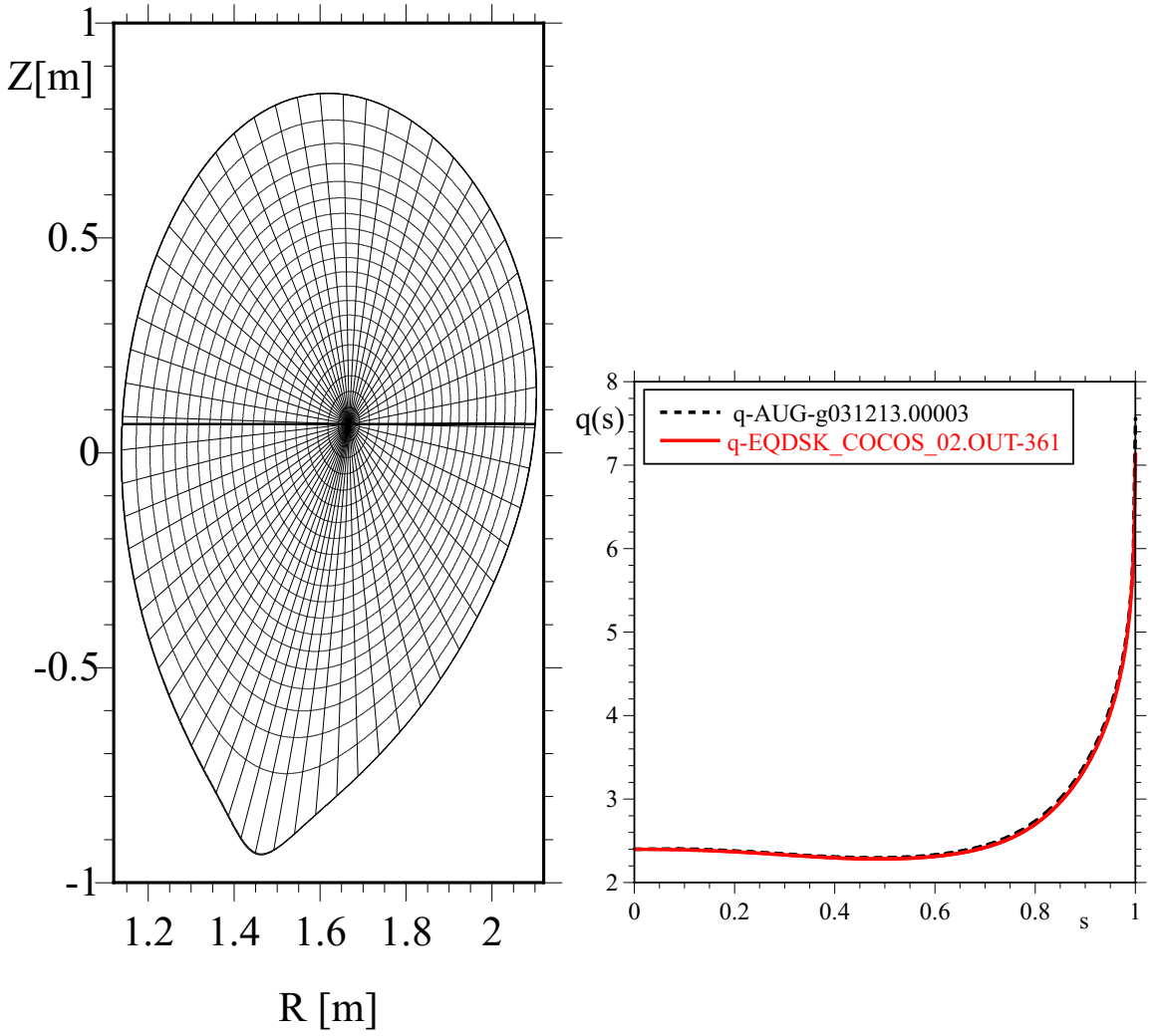


**Figure 1.** Poloidal cross section (left) and safety factor profile $q$ (right) as function of the square root of the normalized poloidal flux for the considered NLED-AUG test case: the black dashed curve is the original q profile from the AUG EQDSK file g031213, and the red solid curve is the q profile after the scaling described in the text.

considered, the peaked on-axis EP density profile (see Fig. 2, red, long-dashed curves), and the peaked off-axis one (see Fig. 2, blue, short-dashed curves), with the Deuterium bulk-ion density profiles defined, for both cases, as $Z_i n_i(s) = n_e(s) - Z_h n_h(s)$ (here $n_i, n_e, n_h$ are the bulk ions, electrons, and EP densities (both bulk ion and EPs are assumed to be Deuterons), respectively, and $Z_i = Z_h = 1$ their electric charge numbers). Maxwellian distribution function will be assumed for the EPs with a constant in radius temperature profile $T_h(s) = 0.093$ [MeV]. Although not strictly required, hybrid codes, as MEGA and HYMAGYC, usually consider some kind of diffusivity, for helping the numerics: the MHD solver of MEGA considers both resistivity $\eta$ and viscosity $\nu$, while the MHD solver of HYMAGYC considers only resistivity. Within the simulations of the present benchmark, normalized resistivity given in terms of the inverse Lundquist

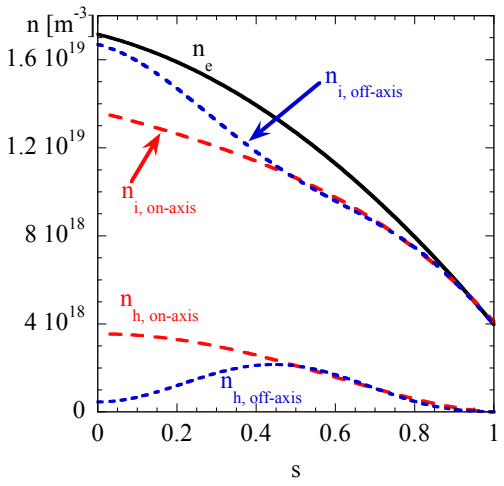


**Figure 2.** Ion densities for the peaked on-axis (red, long-dashed curves), and off-axis (blue, short-dashed curves) EP profiles. Electron density is shown in black, solid curve.

number $S^{-1}_{\rm MEGA} = 5 \times 10^{-7}$ will be used (here, $S_{\rm MEGA} \equiv \mu_0 R_0 (v_{A0}/\eta)$, with $v_{A0}$ the on-axis Alfvén velocity; note that the definition of the normalized resistivity in HYMAGYC differs from the one of MEGA, being $S_{\rm HYMAGYC} \equiv \mu_0 (a^2/R_0)(v_{A0}/\eta)$). A similar value for the normalized viscosity is used in MEGA, being $\nu_{\rm norm} \equiv \nu/(R_0 v_{A0}) = 5 \times 10^{-7}$. In Fig. 3 a sensitivity scan of the codes HYMAGYC and MEGA w.r.t. resistivity (both codes) and viscosity (only MEGA) is presented; the diffusion coefficients have been varied while considering one of the reference cases illustrated in this paper (see Sec. 4.1, peaked-on axis EP radial density profile). Both resistivity and viscosity (and the combined effects of the two, for the MEGA code) add a damping to the EP driven mode observed by both codes (the mode, as it will be shown in Sec. 4.1, will be identified as a Reversed Shear Alfvén mode, RSAE), but their contribution, although clearly observable, for the range of values considered is small when compared to the net growth-rate. Both HYMAGYC and MEGA use, for the adiabatic index, the value $\Gamma = 5/3$ (note that finite values of $\Gamma$ allow for both shear Alfvén and acoustic branches of the Alfvén continuous spectra).

The HYMAGYC MHD solver (which is derived from the full linear, resistive, MHD solver MARS [19]) solves the MHD equations in flux coordinates $(s, \chi, \phi)$ after expanding in Fourier components in the angular coordinates $(\chi, \phi)$ and using finite elements in $s$ (being $s = 0$ on the magnetic axis and $s = 1$ on the plasma boundary). The equilibrium quantities are provided by CHEASE, which solves the Grad-Shafranov equation and maps the solution to the considered flux-coordinate system. In CHEASE, the Jacobian of the transformation from the flux coordinates $(s, \chi, \phi)$ to the Cartesian coordinates is restricted to the form $J = C(s) R^\alpha |\nabla\psi|^\mu$, with $\alpha$ and $\mu$ integers, $R$ the major radius and $\psi$ the poloidal magnetic flux function, and $C(s)$ being obtained by imposing periodicity

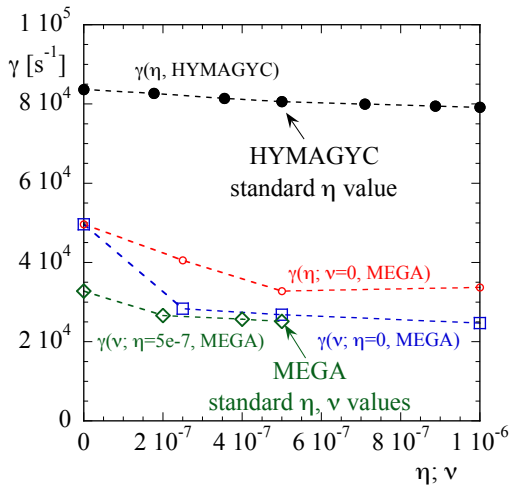


**Figure 3.** Growth-rate vs. resistivity (HYMAGYC and MEGA) and vs. viscosity (MEGA) for one of the reference cases considered in this paper (see Sec. 4.1, peaked-on axis EP radial density profile).

after a poloidal turn. In the following simulations of HYMAGYC, a $\chi$ angle defined by the Jacobian $J \propto R/|\nabla\psi|$ (i.e., $\alpha = 1$, $\mu = -1$, the so-called *equal arc length* coordinate system) will be considered: such a choice of the poloidal angle-like variable $\chi$ usually minimizes the number of Fourier components required to obtain a well converged solution.

Specific code parameters used throughout this benchmark are as follows: HYMAGYC will use, for the field solver module, a radial ($s$) mesh of 180 equally spaced grid points, and a poloidal Fourier spectrum $m = [-3, 13]$, for the considered $n = -1$ toroidal mode; note, however, that the condition of purely real perturbation in the configuration space imposes always to consider a symmetric spectrum of perturbation in the Fourier space $(m, n)$, such that $f_{\mathrm{m,n}} = f^*_{-\mathrm{m},-\mathrm{n}}$, $f$ being a generic perturbed field. Regarding the gyrokinetic module, the numerical markers describing the EP distribution function are evolved in a 3D flux coordinate space $(s, \chi, \phi)$ using a $N_s \times N_\chi = 180 \times 120$ grid points in the $(s, \chi)$ space and a gridless finite-size approach [35] along the $\phi$ direction; typically, we use a number of simulation particles per cell $N_{\mathrm{part/cell}} \equiv N_s \times N_\chi \times N_\phi = 64$, with a number of cells along $\phi$ conventionally fixed to $N_\phi = 8$, thus considering a total number of EP markers $N_{part} = 11,059,200$. Table 1 and Fig. 4 report the results of an example of convergence test with respect to the value of $N_{\mathrm{part/cell}}$. Note that the spread of the values of the growth-rate obtained for the EP driven RSAE is within 0.3% for $N_{\mathrm{part/cell}} \gtrsim 64$.

The number of grid points used for MEGA simulations for the cylindrical coordinates $(R, \phi, Z)$ is $N_R \times N_\phi \times N_Z = 128 \times 16 \times 256$. The numbers of grid points used along the $R$ and $Z$ directions have been chosen in order to have approximately an

| $N_s \times N_\chi \times N_\phi$ | $N_{\mathrm{part/cell}}$ | $\gamma$ $[s^{-1}]$ | $\omega$ [kHz] |
|---|---|---|---|
| 2x2x2 | 8 | 80464 | -127.04 |
| 4x2x2 | 16 | 79730 | -127.21 |
| 4x4x2 | 32 | 80991 | -127.03 |
| 4x4x4 | 64 | 80614 | -127.16 |
| 4x4x8 | 128 | 80697 | -127.19 |
| 4x4x16 | 256 | 80467 | -127.09 |

**Table 1.** Growth-rate vs. the number of energetic particles per cell, $N_{\mathrm{part/cell}}$ obtained by HYMAGYC for one of the reference cases considered in this paper (see Sec. 4.1, peaked-on axis EP radial density profile).

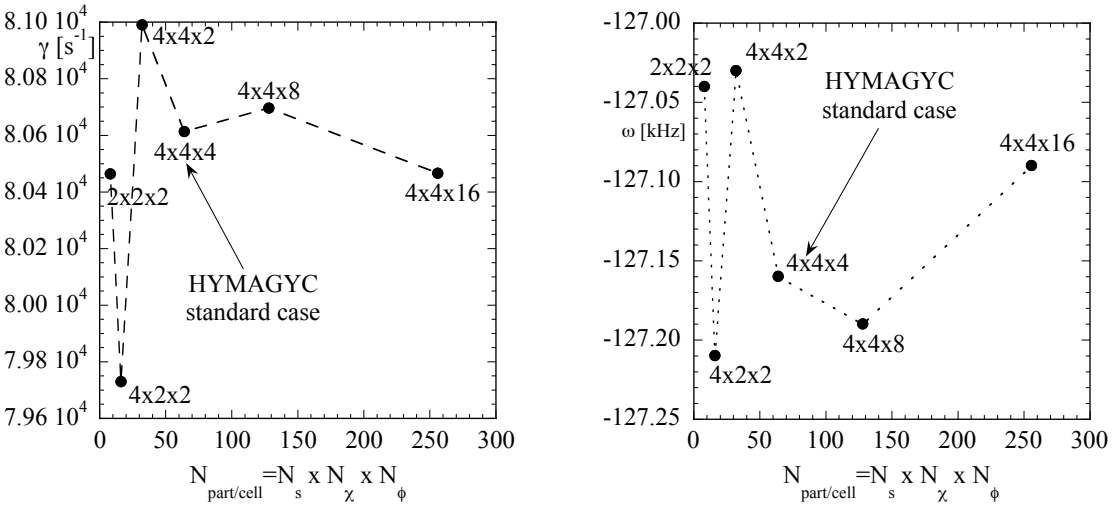


**Figure 4.** Growth-rate vs. the number of energetic particles per cell, $N_{\mathrm{part/cell}}$ obtained by HYMAGYC for one of the reference cases considered in this paper (see Sec. 4.1, peaked-on axis EP radial density profile).

equal spatial resolution along the two directions, considering the elongated cross section (see Fig. 1, left). A sensitivity check for such choice is presented in Table 2 and Fig. 5: note that the maximum spread observed on the growth-rate for the cases considered ($N_R$, $N_Z$ = 128, 256) is within 4% (the frequency for all the cases is $\omega = -132.27$ kHz): thus we consider the default values used in this paper as appropriate to study $n = 1$ modes. The number of marker particles used is $N_{part} = 8,388,608$, i.e., $N_{\mathrm{part/cell}} = 16$. The output of MEGA is in flux coordinates space $(s, \phi, \theta)$, and the Fourier components are chosen by n=[-1,0,1] and m=[0,64].

The number of grid points for ORB5 simulations for the coordinate system $(s, \theta^*, \phi)$ is $N_s \times N_{\theta^*} \times N_\phi = 2000 \times 144 \times 48$ and the number of markers $M$, respectively, for bulk ions, EPs, and electrons are $M_i = M_{EPs} = 3 \times 10^7$, and $M_e = 12 \times 10^7$.

Other parameters and characteristic quantities of the scenarios used for this

| NR | NZ | $\gamma$ $[s^{-1}]$ |
|---|---|---|
| 128 | 128 | 25241.21 |
| 128 | 256 | 25133.90 |
| 256 | 128 | 26210.29 |
| 256 | 256 | 25885.51 |

**Table 2.** Growth-rate vs. the number of grid points $N_R$ and $N_Z$ obtained by MEGA for one of the reference cases considered in this paper (see Sec. 4.1, peaked-on axis EP radial density profile).

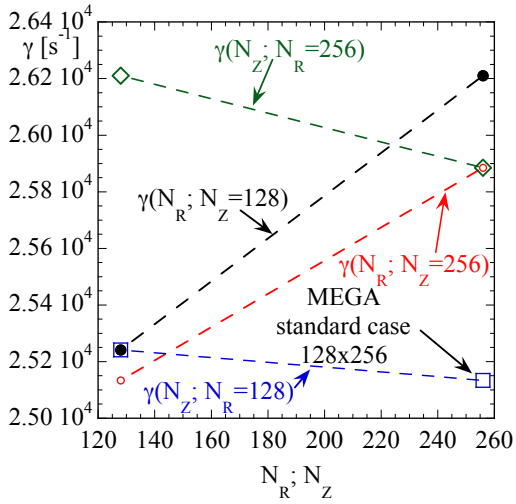


**Figure 5.** Growth-rate vs. the number of grid points $N_R$ or $N_Z$ obtained by MEGA for one of the reference cases considered in this paper (see Sec. 4.1, peaked-on axis EP radial density profile).

benchmark are given in Table 3.

## 3. Characterization of Alfvénic spectra of oscillations in the MHD limit

In order to characterize the equilibrium described in Sec. 2 with reference to the MHD frequency spectra (continuous oscillations and global modes), we have run the hybrid MHD-gyrokinetic codes HYMAGYC and MEGA using the reference on-axis EP density profile but neglecting the EP contribution (i.e., switching off the coupling terms between gyrokinetic and fluid equations and searching for purely MHD solutions), by assigning an arbitrary initial condition and let evolving it in time. In absence of a EP drive term, the perturbed equilibrium is fully stable, apart from a weakly growing mode which can be identified as a tearing mode (see later). As it is well known, initial value simulations of decaying modes pose difficulties in identifying the nature of the oscillations present in the system, mainly because an arbitrary initial condition will excite, typically, a

| Quantity | Value (peaked on-axis case) | Value (peaked off-axis case) | Data definition/Origin |
|---|---|---|---|
| $B_{mag}$ [T] | 2.20811798 | 2.20811798 | EQDSK, magnetic field on the magnetic axis ($R = R_{mag}$) |
| $R_{mag}$ [m] | 1.66599977 | 1.66599977 | EQDSK, magnetic axis major radius |
| $B_0$ [T] | $B_0 = B_{mag}$ | $B_0 = B_{mag}$ | normalization coefficient for the magnetic field |
| $R_0$ [m] | $R_0 = R_{mag}$ | $R_0 = R_{mag}$ | normalization coefficient for the lengths |
| $R_{geo}$ [m] | 1.62 | 1.62 | geometric major radius $(R_{LCMS-max} + R_{LCMS-min})/2$ |
| $a$ [m] | 0.48262 | 0.48262 | minor radius $(R_{LCMS-max} - R_{LCMS-min})/2$ |
| $\epsilon_0$ | 0.297898 | 0.297898 | inverse aspect ratio $(a/R_{geo})$ |
| $n_{e0}$ $[10^{20}/m^3]$ | 0.171587 | 0.171587 | on-axis electron density |
| $n_{h0}$ $[10^{20}/m^3]$ | 0.03552 | 0.00458182 | on-axis EP density |
| $n_{i0}$ $[10^{20}/m^3]$ | 0.136067 | 0.16700518 | on-axis bulk ion density (from $n_i = n_e - n_h$) |
| $n_{h0}/n_{i0}$ | 0.261048 | 0.0274352 | EP density/bulk ion density |
| $m_i/Z_i$ | 2/1 | 2/1 | bulk ion mass/charge (D) (in units of proton mass/electron charge) |
| $m_h/Z_h$ | 2/1 | 2/1 | EP mass/charge (D) (in units of proton mass/electron charge) |
| $m_h/m_i$ | 1 | 1 | mass ratio (EP/bulk ion) |
| $T_{h0}$ [MeV] | 0.093 | 0.093 | on-axis EP Temperature (constant on radius), Maxwellian distribution |
| $v_{A0}$ [m/s] | $9.22757 \times 10^6$ | $8.32911 \times 10^6$ | on-axis Alfvén velocity: $v_{A0} = 2.18 \times 10^6\ B_{mag}[\mathrm{T}]/\sqrt{m_i n_{i0}[10^{20}/m^3]}$ |
| $\tau_{A0}$ [s] | $1.80546 \times 10^{-7}$ | $2.00021 \times 10^{-7}$ | on-axis Alfvén time: $\tau_{A0} \equiv R_0/v_{A0}$ |
| $\omega_{A0}$ [rad/s] | $5.53876 \times 10^6$ | $4.99947 \times 10^6$ | $\omega_{A0} = 1/\tau_{A0}$ |
| $v_{h,th0}$ [m/s] | $2.1111 \times 10^6$ | $2.1111 \times 10^6$ | $v_{h,th0} \equiv \sqrt{T_{h0}/m_h} = 9.79 \times 10^6 \sqrt{T_{h0}[MeV]/m_h}$ |
| $v_{h,th0}/v_{A0}$ | 0.228782 | 0.253461 | on-axis EP thermal velocity/on-axis Alfvén velocity |
| $\Omega_{h0}$ [rad/s] | $1.057688 \times 10^8$ | $1.057688 \times 10^8$ | on-axis EP gyrofrequency: $\Omega_{h0} = 9.58 \times 10^7 Z_h B_0[\mathrm{T}]/m_h$ |
| $\rho_{h0}$ [m] | 0.0199221 | 0.0199221 | on-axis EP Larmor radius $\rho_{h0} = v_{h,th0}/\Omega_{h0} = 0.102\sqrt{m_h T_{h0}[MeV]}/(Z_h B_0[T])$ |
| $\rho_{h0}/R_0$ | 0.011958 | 0.011958 | on-axis EP Larmor radius/$R_0$ |
| $\rho_{h0}/a$ | 0.041279 | 0.041279 | on-axis EP Larmor radius/$a$ |

**Table 3.** AUG benchmark test case parameters.

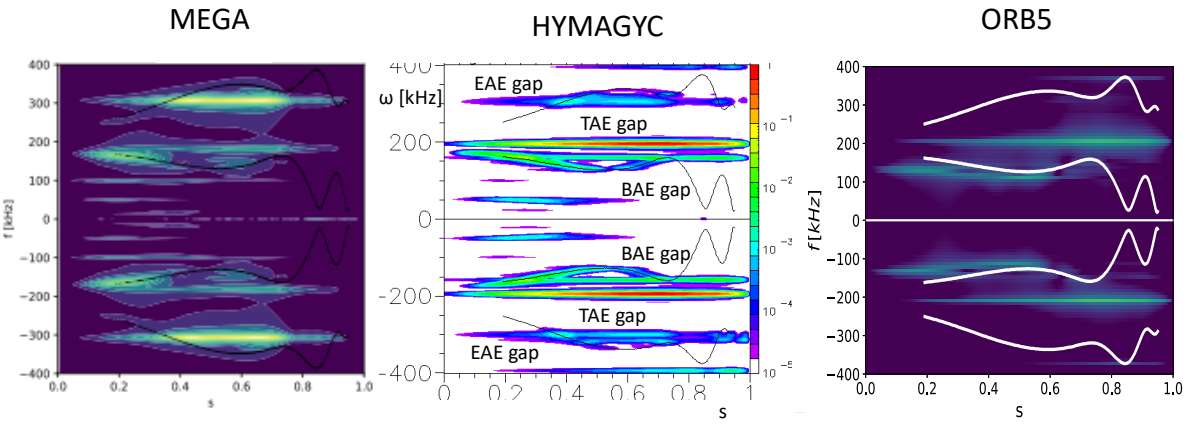


**Figure 6.** Frequency spectra in the MHD limit for MEGA (left), HYMAGYC (centre), and ORB5 (right). Logarithmic color scale is used for the intensity of the e.s. field $|\varphi(s,\omega)|^2$. Shear Alfvén coutinuous spectra are also shown using black continuous lines for the MEGA and HYMAGYC spectra, and as white continuous lines for the ORB5 spectra, as obtained by the FALCON code. In the central frame the main gaps are also indicated for reference.

large variety of local as well as global oscillations. When unstable modes are present, indeed, the difficulties are mitigated by the fact that, waiting a sufficient time, the fastest growing mode will dominate on all the other oscillations, thus making its identification and study much easier (at least during a linear growing regime). In order

to analyze and identify the different type of oscillations admitted by this equilibrium, it is instructive to Fourier analyze in time the results of the simulations, as shown in Fig. 6, where the frequency spectra $|\varphi(s,\omega)|^2$ of the electrostatic field components $\varphi_{\mathrm{m,n}}(s,t)$ are illustrated for MEGA, HYMAGYC and ORB5. In Fig. 6 also the shear Alfvén continuous spectra are shown for reference (plotted using black continuous lines for the MEGA and HYMAGYC spectra, and as white continuous lines for the ORB5 spectra), as obtained by the FALCON code [36] in the limit of slow-sound approximation [37] (acoustic Alfvén continua as obtained by FALCON, although present in the system, are not shown for the sake of clarity of the figures). The frequency spectrum is almost perfectly symmetric w.r.t. the $\omega$ sign. A variety of oscillations are observed, almost all of them being damped (apart from the tearing mode). We will refer, in the following, to lower and upper shear Alfvén continuous spectra as the ones with lower and higher values of *absolute* frequencies, respectively. To better enlighten the different global modes and local oscillations observed in the simulations, a logarithmic color scale representing the amplitude of the power spectra has been used in Fig. 6. All the three codes clearly show few dominant global (radially extended) modes localized in frequency within the toroidal Alfvén gap (TAEs); the richness of the spectra is evident from the results of the two hybrid codes MEGA and HYMAGYC, where also few peaks mainly localized on several Slow Magneto-acoustic continua, in the frequency range of beta induced Alfvén Eigenmode (BAE) and beta induced Alfvén acoustic eigenmode (BAAE) gaps (in the frequency range $|\omega| \lesssim 100$ [kHz] and for $0 \lesssim s \lesssim 0.6$ ), are observed. Note that these low frequency modes are only observed by HYMAGYC and MEGA, which are hybrid MHD-Gyrokinetic codes, whereas ORB5 do not observe any relevant oscillation in this portion of the spectrum, in agreement with the expectation that this region of the spectrum is strongly damped in full gyrokinetic codes. Moreover, HYMAGYC observes alsoa mode lying above the upper toroidal Alfvén continuous spectrum, within the ellipticity Alfvén gap (EAE). Also a clear evidence of local oscillations superimposed to the lower toroidal Alfvén continuous spectrum are observed, showing that the codes well represent the continua oscillations.

The identification of the damping rate or growth rate of various modes excited by the initial condition, as well as their global or local nature is greatly facilitated by executing a series of frequency spectra on a time series shorter than the full simulation, and moving these time series from the beginning of the simulation toward the end (the application of standard techniques to treat frequency spectra on data series, as Hanning function [38] and buffering [39] of the signals could help in refining and clarifying the results). Keeping track of the time evolution of the characteristics of the relative maxima (i.e., their amplitudes $\mathrm{Amp}_{\mathrm{rel.\ max.,j}}(t)$, their their frequencies $\omega_{\mathrm{rel.\ max.,j}}(t)$, and radial positions (i.e. the $s$ coordinates) $s_{\mathrm{rel.\ max.,j}}(t)$, with $j$ indicating the order of the maxima), it is possible, within a single simulation, to gain insight about damping and growth rates of the oscillations and, eventually, identify them as global modes or oscillations belonging to the different continua. In Fig. 7 an example of such an analysis is shown (and which is routinely done for the HYMAGYC simulations), with reference

to the negative frequency portion of the power spectra shown in Fig. 6 and relative to the HYMAGYC simulation, with the identification of the most relevant global modes observed (see Fig. 7a): these are radially extended structures which oscillate at the

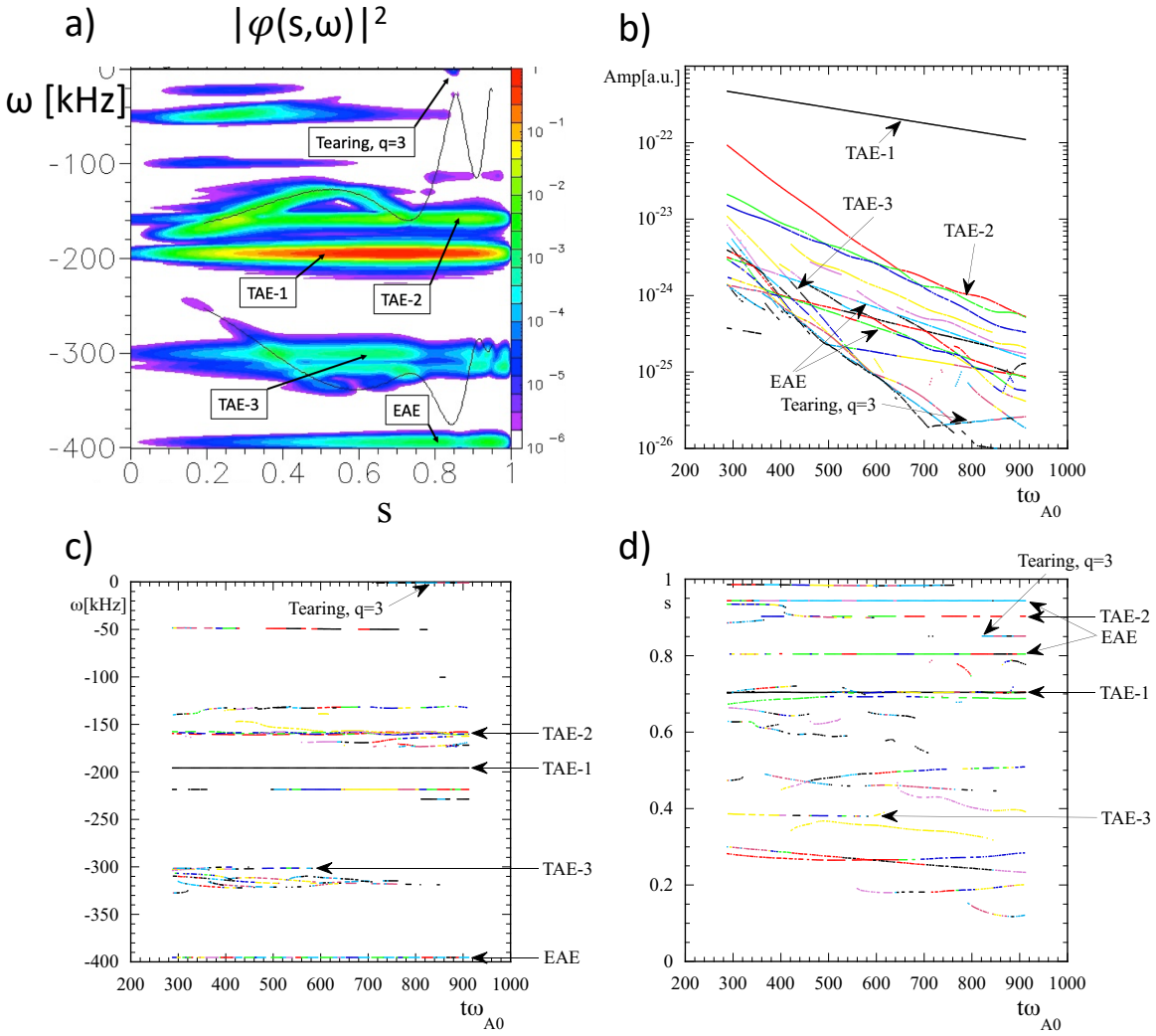


**Figure 7.** Frequency power spectra of the e.s. field $|\varphi(s,\omega)|^2$ for the HYMAGYC simulation shown in Fig. 6 (only negative portion of the frequency plane), with the identification of the dominant modes observed (a). Amplitude (b), frequency (c), and radial position (d) versus time of the relative maxima of the frequency spectra of the HYMAGYC simulation shown in (a). A fixed sequence of colors (related to the values of the $\mathrm{Amp}_{\mathrm{rel.\ max.}}(t)$: black the highest value, red the second highest, and then green, blue, yellow, violet and cyan, and then cycled) is used for each time; the same colors of the dots are used also for the other plots (c) and (d), to help the identification of the modes.

same frequency through all their radial extension, and which grow/decay in time with an almost unchanged radial shape. Curves that in the $\mathrm{Amp}_{\mathrm{rel.\ max.,j}}(t)$ plot do not show a rectilinear behaviour, i.e., an exponential decay, typically belong to local, continua oscillations. As an example, the dominant mode observed in Fig. 7a, which has its

| mode | $\gamma_{\text{HYMAGYC}}$ $[s^{-1}]$ | $\omega_{\text{HYMAGYC}}$ [kHz] | $\gamma_{\text{MEGA}}$ $[s^{-1}]$ | $\omega_{\text{MEGA}}$ [kHz] | $\gamma^{\dagger}_{\text{ORB5}}$ $[s^{-1}]$ | $\omega^{\dagger}_{\text{ORB5}}$ [kHz] |
|---|---|---|---|---|---|---|
| Tearing-q=3 | 4080.2 | 0.0 | | | | |
| TAE-2 | -14594.6 | -159.2 | -45060.0 | -171.9 | $\approx -10000.$ | -146. |
| TAE-1 | -6455.3 | -195.8 | -36057.0 | -185.2 | $\approx -6000.$ | -206. |
| TAE-3 | -29484.2 | -301.4 | -30120.0 | -304.2 | | |
| EAE | -13542.3 | -395.8 | | | | |

**Table 4.** Growth rates $[s^{-1}]$ and real frequencies [kHz] of some of the modes observed in Fig. 6, corresponding to the HYMAGYC, MEGA and ORB5 purely MHD simulations, on-axis AUG reference case. ($^{\dagger}$) Note that for the ORB5 simulation, $n_i = n_e$ has been considered, whereas both HYMAGYC and MEGA assume $n_i = n_e - n_{h,\text{on-axis}}$, with $n_{h,\text{on-axis}}$ the peaked on-axis EP density, while neglecting the EP contribution in the fluid equations.

maximum (red colored contour) at frequency $\omega \approx -196$ kHz and located at $s \approx 0.7$, is identified in Fig. 7b, 7c, 7d as a Toroidal Alfvén Eigenmode (there labelled as "TAE-1"), which is weakly damped because of the small amount of resistivity used in these simulations: its damping rate $\gamma \approx -6455$ s$^{-1}$ is easily evaluated from the slope of the black dots in Fig. 7b, at the highest amplitude values; moreover, the constancy in time of the corresponding frequency and radial curves, together with its corresponding shape in the frequency spectra Fig. 7a, let us identify this maximum as an eigenmode of the system.

Note that also a weakly growing mode is reported for the simulation of HYMAGYC, which is radially localized at $s \approx 0.85$, at the radial position were $q(s) = 3$, thus being identified as a tearing mode ($m = 3, n = -1$). In Table 4 also few modes identified in a similar simulation by ORB5 are shown, in quite good agreement with the two hybrid codes of this benchmark, namely, HYMAGYC and MEGA; the only difference w.r.t. the hybrid codes being that the bulk ion profile for the ORB5 simulation must be $n_i = n_e$, quasi-neutrality being mandatory for fully gyrokinetic codes, and the different bulk ion density profile reflecting, as a consequence, in a slightly different shear Alfvén frequency spectra.

## 4. Linear results of the benchmark

In this Section, the linear stability results obtained by the three codes is presented, comparing the radial structure of the most unstable modes observed in the simulations and their frequency power spectra of both the peaked on-axis and off-axis EP density profiles. In particular, the results of simulations for the nominal values will first be shown in Sec. 4.1, and the dependence of the simulation results on the intensity of the drive when varying, separately, the EP density (see Sec. 4.2) and the EP temperature (see Sec. 4.3) will then be presented; moreover, some considerations on the growth rate of the observed modes will be also given.

### *4.1. Nominal cases comparison*

In Fig. 8 the results of the three codes for the two reference cases (peaked on-axis and off-axis EP density profiles) are shown: in both cases, for all the three codes considered, a mode driven by the EP is observed. Let's consider, first, the results for the peaked on-axis EP density profile (Fig. 8, left column): after an initial transient phase of

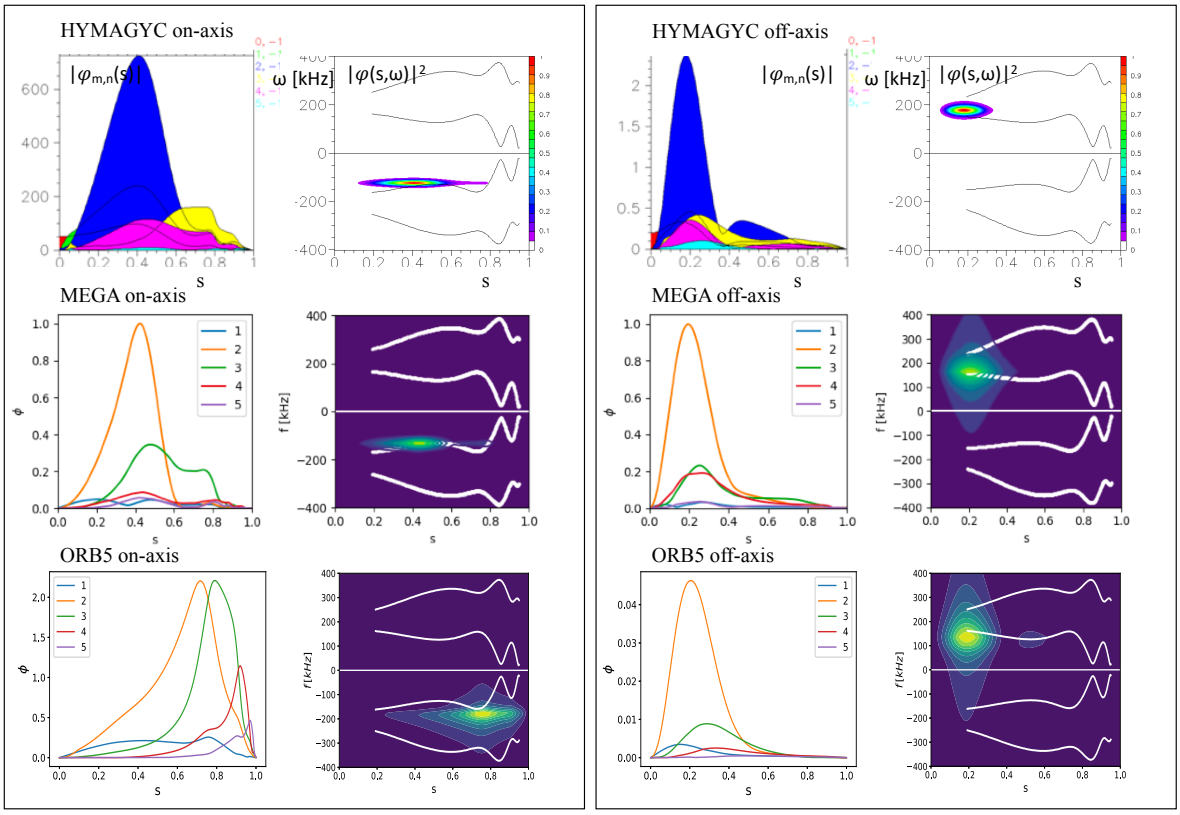


**Figure 8.** Comparison between the results obtained for HYMGYC (top row), MEGA (centre row), ORB5 (bottom row), for the two AUG nominal cases: peaked on-axis EP density profile (left column) $n_{h0}/n_{i0} = 0.261$, $T_h = 0.093$ MeV, and peaked off-axis EP density profile (right column) $n_{h0}/n_{i0} = 0.0274$, $T_h = 0.093$ MeV. The radial profiles for different poloidal Fourier components of the e.s. potential $\varphi(s)$, and its power frequency spectra are plotted for each case (linear color scale).

the simulations, both HYMAGYC and MEGA observe, as the most unstable one, a mode located around $s \approx 0.4$, with a dominant $m = 2$ poloidal Fourier component for the electrostatic field $\varphi$, and located around $\omega \approx -130$ kHz in frequency, i.e., with a frequency slightly lower (in absolute value) than the lower shear Alfvén continuous spectrum. These observations, together with the fact that its radial location is quite close to the minimum $q$ value (see Fig. 1, right), suggest that this mode is a so-called Reversed Shear Alfvén Eigenmode (RSAE). The mode is driven, both in HYMAGYC and MEGA simulations, mainly by the co-passing EPs (see the Fig. 9, where the power exchange between energetic particles and wave is shown in the normalized parallel velocity and magnetic moment plane). On the other side, the result of ORB5 shows,

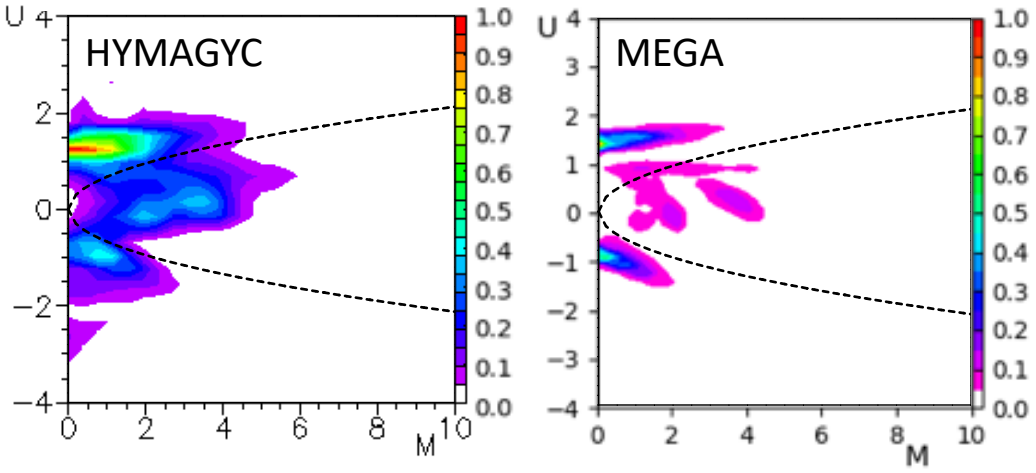


**Figure 9.** Wave-particle power exchange in the plane $[U, M]$ for the nominal case parameter, peaked on-axis EP density profile. Here $U$ is the normalized (to the EP thermal velocity) EP parallel velocity, and $M$ is the normalized (to $T_h/\Omega_{h0}$, with $\Omega_{h0}$ the on-axis EP cyclotron frequency) EP magnetic moment. HYMAGYC result is shown on the left, and MEGA result on the right; red pattern indicates maximum power exchange from EPs to the wave. Also the approximate boundary between trapped and circulating particles (co-passing for positive $U$ values, counter-passing for negative $U$ ones) is drawn, corresponding to the radial region where the mode is maximum ($s \approx 0.4$).

for the most unstable mode, a more externally localized structure ($s \approx 0.7$) dominated by $m = 2, 3$, and localized, in frequency, close to the lower (in absolute value) tip of the toroidal gap, $\omega \approx -200$ kHz. When considering the peaked off-axis EP density profile, on the other side (Fig. 8, right column), all the three codes show a very good agreement. In particular, all of them observe a mode located, radially, close to the magnetic axis ($s \approx 0.2$), dominated by a $m = 2$ poloidal Fourier component, and located, in frequency, within the toroidal gap and with opposite sign w.r.t. to the previous, peaked on-axis, case. Note that the radial localization correspond to the EP density profile characterized by a positive radial gradient (see Fig. 2), i.e., with opposite sign w.r.t. to the peaked on-axis, monotonically decreasing, EP density profile (and, thus, with opposite sign of the diamagnetic frequency of the EPs driving term, which is $\propto \omega_h^*$ [40]). Some more insight on the results of the simulations, and, in particular, regarding the discrepancies observed, for the peaked on-axis EP density profile case, among ORB5 on one side, and HYMAGYC and MEGA on the other side, can be gained by comparing the results of the simulations performed by varying two parameters, namely, the on-axis EP density $n_{h0}$ and temperature $T_{h0}$, as will be shown in the next sub-Secs. 4.2 and 4.3.

### *4.2. Energetic particle density scan*

In this Section the results of varying the EP density w.r.t. the reference case values are presented. The attention will be focused on the growth rate of the modes observed in the simulations, and, possibly, the results will be connected to the ones presented in the so-called MHD limit presented in Sec. 3. Indeed, varying the EP density will modify, accordingly, the intensity of the EP drive, while keeping unchanged the EP motion, i.e., their resonances and characteristic frequencies. Note that, in order to correctly satisfy the quasi-neutrality requirement of ORB5, the bulk ion density profile will be recomputed accordingly, for each simulation: this imply, as a consequence, that the $\omega_{A0}$ value and Alfvén shear continua will slightly change for each different value of $n_{h0}$ considered in the simulations. Figure 10 shows the results of the EP density scan for the on-axis EP density profile, ranging from the MHD limit ($n_{h0}/n_{i0} = 0$) to the nominal value (indicated by vertical dashed lines in the frames of Fig. 10) and beyond. HYMAGYC observes two different modes, depending on the EP density range:

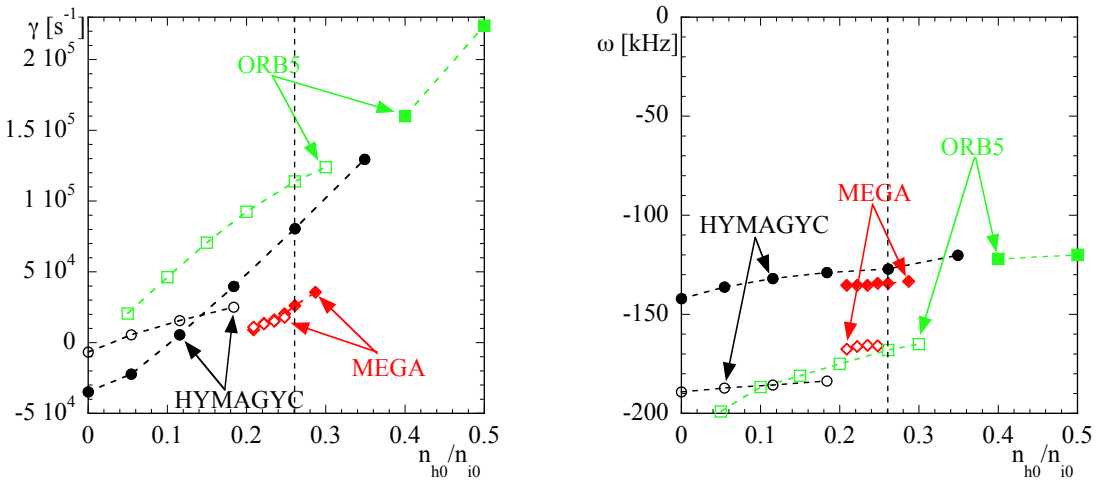


**Figure 10.** Energetic particle density scan for the AUG on-axis EP density profile: growth rates (left frame) and frequencies (right frame). Black circles refer to HYMAGYC results, red diamonds to MEGA, and green squares to ORB5, with closed symbols indicating RSAEs and open symbols to TAEs. The dashed black vertical lines refer to the nominal value of $n_{h0}/n_{i0}$.

for small values of $n_{h0}/n_{i0}$ the most unstable (or less damped) mode is a mode radially located at $0.6 \lesssim s \lesssim 1$, in correspondence with the external part of the toroidal gap ($\omega \approx -180$ kHz), which made the identification of this mode as a TAE (see Fig. 11 (left column, top frames). Note that the damping rate and real frequency of this TAE in the limit $n_{h0}/n_{i0} = 0$ are almost the same of the less damped MHD mode described in Sec. 3, although the simulations have slightly different bulk ion densities ($n_i = n_e$ here, whereas $n_i = n_e - n_{h,\text{nominal}}$ was use in Sec. 3). In a more internal radial region, centered

radially around $s \approx 0.4$ and with frequency $\omega \lesssim -140$ kHz, a second mode, a RSAE, is clearly observed in the frequency spectra plot of Fig. 11 (left column, top right frame), which is sub-dominant w.r.t. the TAE; the presence of the RSAE is also observed in the radial profile of the e.s. potential Fourier component $|\varphi_{\mathrm{m,n}}(s)|$ with $m = 2$, where a local peak is observed at $s \approx 0.45$. For higher EP density values, $n_{h0}/n_{i0} \gtrsim 0.15$, the RSAE growth rate become larger that the TAE mode, i.e., it becomes the dominant mode, and, eventually, it is the only observable mode in the HYMAGYC simulations (Fig. 11 (right column, top frames)). The separation between TAE and RSAE modes is clearly observed in Fig. 10 (right frame), showing the dependence of the frequency on the EP density, and where the open symbols are used for the TAEs and the closed symbols for the RSAEs. Similar results are observed by MEGA, with close values to the ones

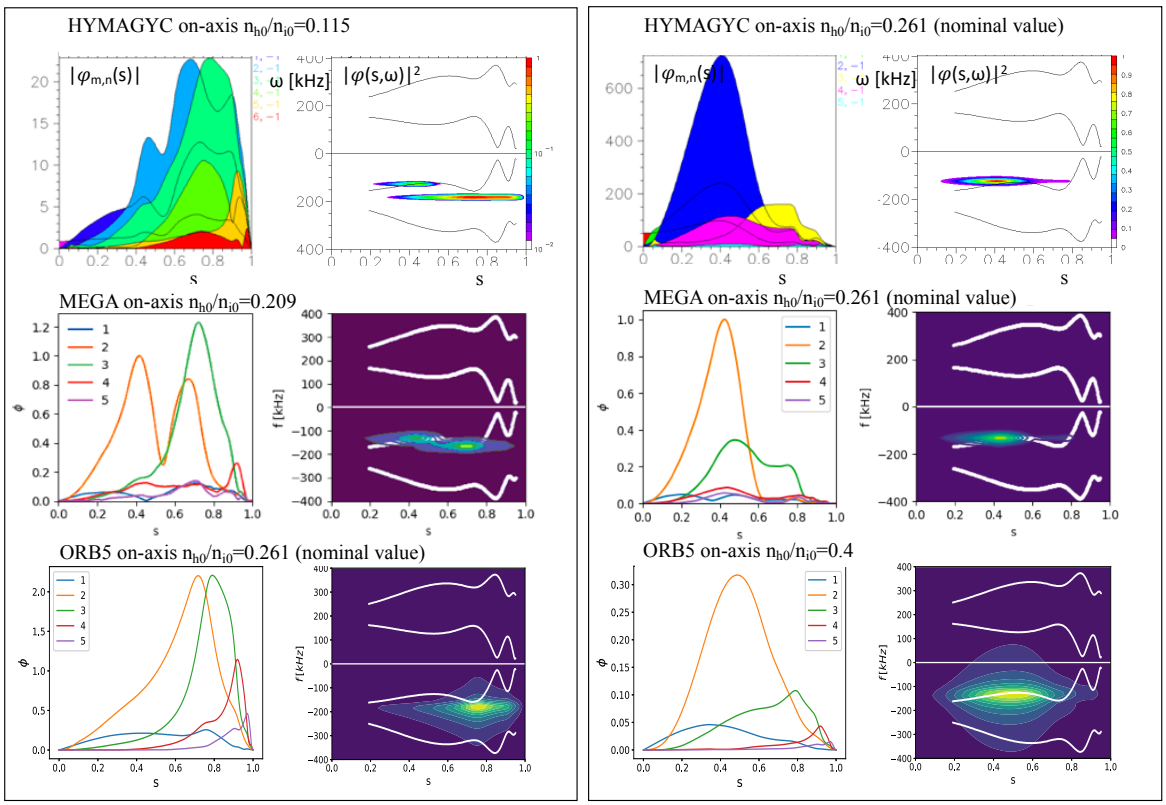


**Figure 11.** TAE solution (left) and RSAE solution (right) as obtained by HYMAGYC (top), MEGA (middle), and ORB5 (bottom) at "low" values of EP density (left column), and "high" density (right column). Note that the values of $n_{h0}/n_{i0}$ varies for each plot; note also that some of the plots shown in this Figure are the same of Fig. 8 and are reported here for the ease of the reader.

observed by HYMAGYC, for both the frequencies and spatial location of the modes, but definitely smaller growth rate values (see Fig. 10 (left frame)). In Fig. 11 (left column, middle frames) a simulation of MEGA for a value of $n_{h0}/n_{i0} = 0.209$ is shown: for such a value, the two modes, i.e., the external TAE, and the more central RSAE are observed, with similar amplitudes among each other, being their growth rates very similar (see Fig. 10 (left frame)). Also ORB5 observes the two different modes shown by

HYMAGYC and MEGA, but the range of EP density where the RSAE dominates over the TAE is, in this case, above the nominal density case (i.e., for $n_{h0}/n_{i0} \gtrsim 0.4$) (see Fig. 10 and Fig. 11 (left and right columns, bottom frames)). Moreover, growth rates observed by ORB5 are, generally speaking, larger that the ones observed by HYMAGYC and MEGA.

Having analyzed with some more detail the behaviour of the three codes w.r.t. EP density, we can draw some conclusions on the main differences exhibited, i.e., the different values of the growth rate, and the EP density threshold at which the RSAE overcomes the TAE solution. Indeed, extrapolating the growth (or damping) rate toward the origin (i.e., to the MHD limit) it is possible to confirm the results already observed in Sec. 3, namely, MEGA code shows, generally speaking, a stronger damping w.r.t. HYMAGYC and ORB5 (this consideration is, of course, consistent with the fact that MEGA runs with finite resistivity and viscosity, whereas HYMAGYC consider only finite resistivity, and that the numerical scheme used to solve field equations in MEGA could also have larger numerical diffusion than HYMAGYC; moreover, ORB5 do not consider neither resistivity nor viscosity terms, as already stated before). Moreover, the TAE solution found by MEGA exhibits a real frequency closer, in absolute value, to the lower tip of the toroidal gap than the real frequency found by HYMAGYC: this fact is consistent with a likely higher radiative damping [41, 42] felt by MEGA. On the other side, the two hybrid codes, HYMAGYC and MEGA, exhibit a dependence of the TAE growth rate w.r.t. the EP density quite similar (almost the same slope), whereas ORB5 exhibits a quit larger dependence, which tends to decrease as the EP density increases and, correspondingly, the real frequency of the mode becomes closer and closer to the lower tip of the toroidal gap shear Alfvén continua, and, thus, likely increases the damping. On the other hand, considering the RSAE solution, HYMAGYC and ORB5 observe almost the same EP density dependence (very similar slope and values of the growth rate, see Fig. 10 (left frame), and extrapolation to zero EP density); also the RSAE solution found by MEGA is not much different, exhibiting a little smaller slope and little higher extrapolation to zero EP density; indeed, also the real frequency solutions observed by the three codes are quite similar (see Fig. 10 (right frame)). It is possible to conclude that the relatively large difference of the EP density threshold at which each code observes the RSAE growth rate to overcome the TAE solution it is likely to depend on the details of various damping considered in the simulations (e.g., finite resistivity, finite viscosity, radiative damping [41, 42], continuum damping [43] and different numerical dissipation), and on the differences of the model considered, i.e., hybrid MHD-gyrokinetics vs. fully gyrokinetics.

Figure 12 shows the results of the EP density scan for the peaked off-axis EP density profile. In this case, all the three codes observe, as the dominant mode, a TAE located close to the magnetic axis, with a frequency well within the toroidal gap, at $\omega \approx 150$ kHz. The radial profile of the Fourier components are very similar, all dominated by a $m = 2$ poloidal Fourier component; the growth rates obtained by ORB5 are larger that the ones obtained by HYMAGYC and MEGA; for this case, MEGA obtains slightly

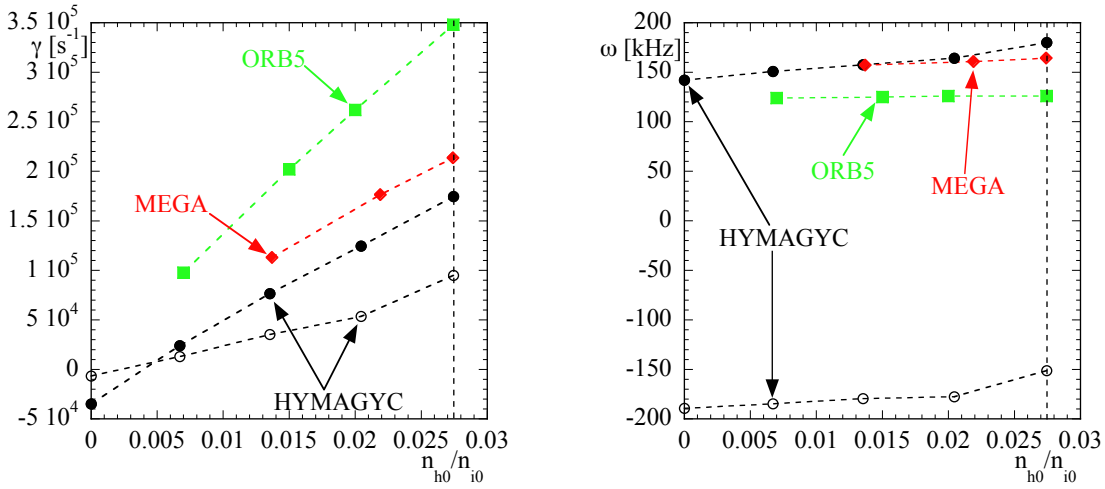


**Figure 12.** Energetic particle density scan for the AUG off-axis EP density profile: growth rates (left frame) and frequencies (right frame). Black circles refer to HYMAGYC results, red diamonds to MEGA, and green squares to ORB5, with closed symbols indicating core-localized TAEs and open symbols the external TAEs. The dashed black vertical lines refer to the nominal value of $n_{h0}/n_{i0}$.

larger growth rates than HYMAGYC. Note that HYMAGYC, with a careful analysis of the frequency power spectra, is able to recognize also a sub-dominant, more external mode, characterized by a negative frequency $\omega \approx -200$ kHz, and located within the toroidal gap, at the radial position $s \approx 0.7$ (see Fig. 13). Note that this mode is very similar to the one observed in the previous, peaked on-axis EP density profile case: indeed, the nominal EP density profiles of the peaked on-axis and of the peaked off-axis EP density profiles almost overlap each other in the external, $s \gtrsim 0.5$, region (see Fig. 2).

### *4.3. Energetic particle temperature scan*

In Figure 14 the results of the simulations varying the EP temperature are shown, both for the peaked on-axis (top plots) and peaked off-axis (bottom plots) EP density profiles, while considering, for each case, the nominal EP density values. The dependence of the growth rate and frequency obtained by the three codes is very similar, with the growth rate increasing almost linear with $T_h$ for the peaked on-axis EP density case (see Fig. 14 top, left), and weaker than linear with $T_h$ for the peaked off-axis EP density case (see Fig. 14 bottom, left). Note, also, that for the peaked on-axis EP density profile case, ORB5 observes, at lower values of $T_h$ ($T_h \lesssim 0.093$ keV), a TAE mode radially localized at the external part of the toroidal gap (indicated in Fig. 14 top figures, with open green squares), whereas HYMAGYC and MEGA observe a RSAE (see also the Sec. 4.2, where a similar behaviour of ORB5 w.r.t. HYMAGYC and MEGA was observed for

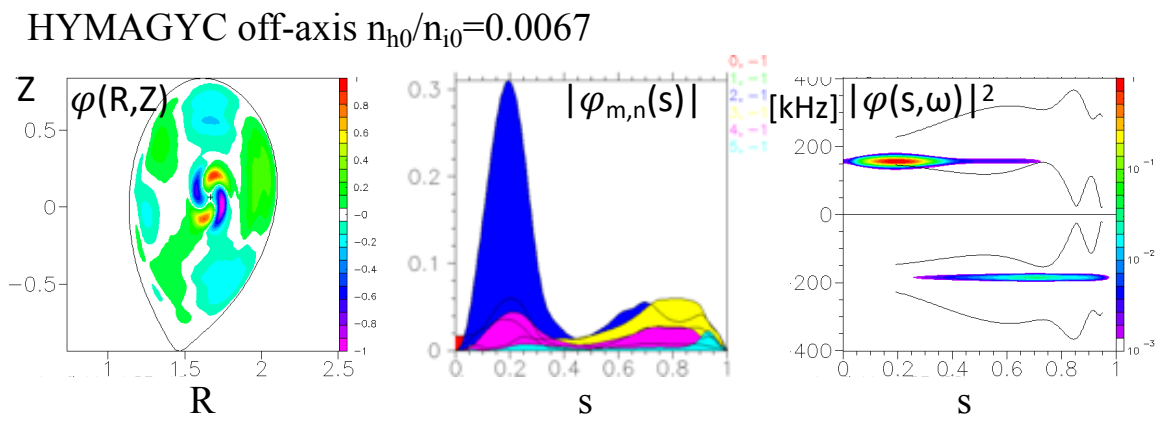


**Figure 13.** HYMAGYC: peaked off-axis Energetic Particle density profile, with $n_{h0}/n_{i0}$=0.0067: e.s. field structure $\varphi(R,Z)$ in the poloidal plane $\phi = 0$ (left), radial profiles of the Fourier components $|\varphi_{\mathrm{m,n}}(s)|$ (centre), and frequency power spectra $|\varphi(s,\omega)|^2$ (right). The dominant core localized TAE ($s \lesssim 0.4$), with preeminent $m = 2$ poloidal Fourier component is observed in the central region, with a positive real frequency; in the external region ($s \gtrsim 0.4$) it is also present the sub-dominant external TAE, with a preeminent $m = 3$ poloidal Fourier component and a negative real frequency (i.e., with opposite sign w.r.t. the dominant internal mode).

weaker drive because of small $n_{h0}/n_{i0}$). On the other hand, for higher values of $T_h$ ($T_h \gtrsim 0.11$ MeV), and, thus, for stronger EP drive, also ORB5, as the other two codes, observes a RSAE as the dominant mode (indicated, in Fig. 14 (top figures), with filled green squares): indeed, the different nature of the mode observed by ORB5 at higher $T_h$ is evident when noting the discontinuity in the frequency values (filled vs. open green squares in Fig. 14 top right figure).

It has to be noted, also, that, for the peaked off-axis EP density profile (Fig. 14 bottom figures), the code HYMAGYC is able to observe also the sub-dominant TAE mode (as in the EP density scan), located radially in the external part of the TAE gap (open circle symbols), which behaves similar to the other dominant, internal TAE, as $T_h$ is varied. As a general consideration, the dependence of the growth rate, w.r.t. the EP temperature, is similar among the three codes, ORB5 showing typically a stronger net growth rate than the two hybrid codes HYMAGYC and MEGA.

## 5. Conclusions

In this paper the two hybrid MHD-gyrokinetic codes HYMAGYC and MEGA, and the full gyrokinetic code ORB5 have been benchmarked, in the linear regime, by studying the EP driven Alfvénic modes in a realistic equilibrium, namely, the fully shaped NLED-AUG test case [14]; the two variants of EP density profile, namely, the peaked on-axis and the peaked off-axis ones have been analyzed, while considering perturbations with toroidal mode number $n = -1$. Particular care has been dedicated to use as

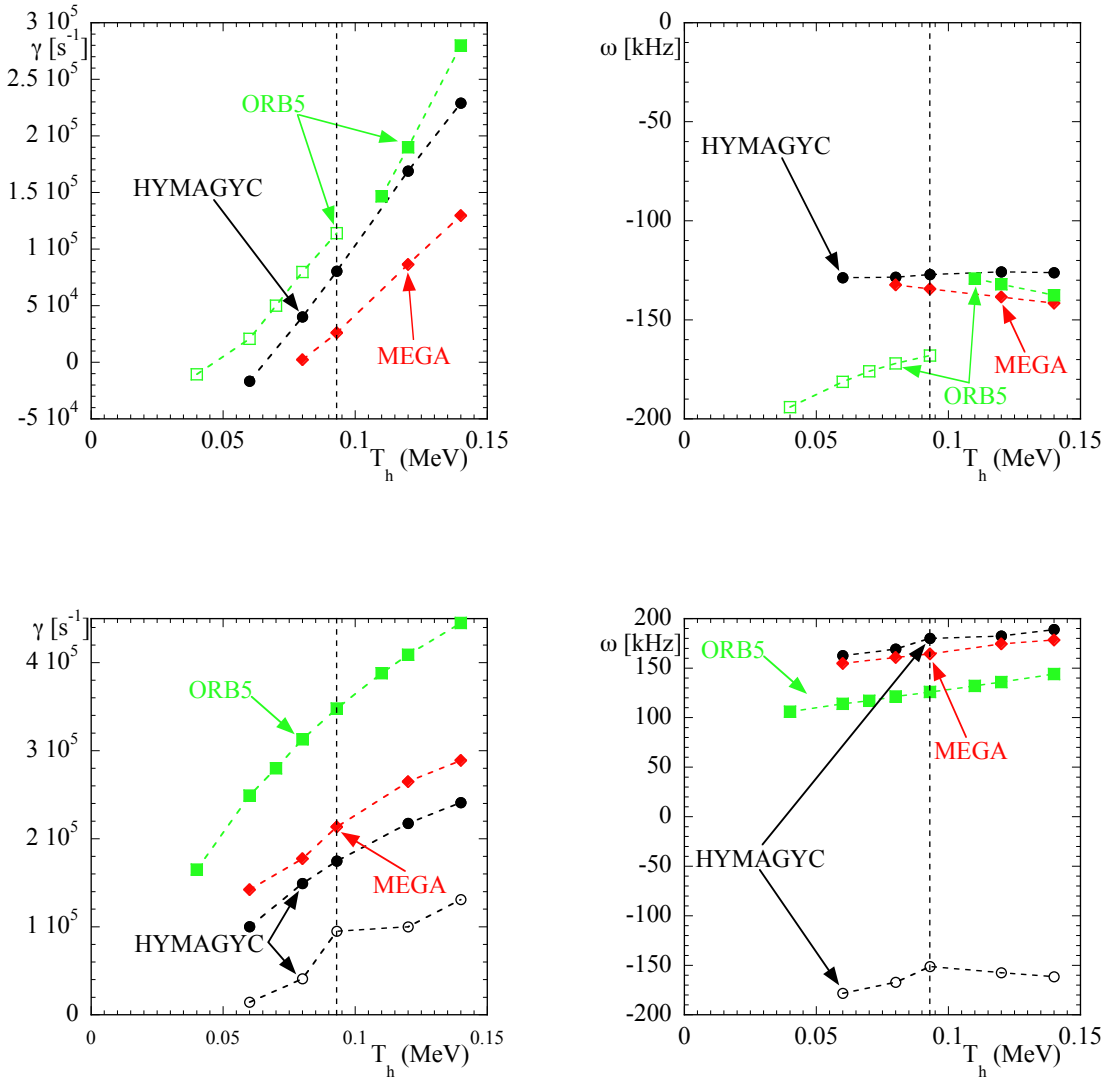


**Figure 14.** Growth rates (left column) and frequencies (right column) vs. $T_h$ for the on-axis (top row) and off-axis (bottom row) EP density profiles. Black circles refer to HYMAGYC results, red diamonds to MEGA, and green squares to ORB5. The dashed black vertical lines refer to the nominal value of $T_{h0}$.

closest as possible equilibrium data and code parameters. In particular, a same high resolution EQDSK version of the NLED-AUG case has been used, after re-computing the equilibrium with the code CHEASE [16], starting from the original AUG-NLED EQDSK file. Input parameters and model dependent data have been kept as close as possible between the codes: e.g., when performing the EP density scan, the bulk ion density has been consistently calculated by assuming quasi-neutrality, as imposed by ORB5, also for the hybrid codes. To help numerical convergence, both HYMAGYC and MEGA have considered finite resistivity; MEGA considers also finite viscosity; both the

hybrid codes considered finite adiabatic index $\Gamma = 5/3$.

Purely MHD spectra of oscillation have been first compared, executing runs without energetic particles drive contribution. The richness of the oscillations and global modes of the NLED-AUG equilibrium test case is already shown by such MHD analysis, which enlighten Alfvén continua oscillations and a variety of global Alfvén eigenmodes, as, e.g., TAEs and EAEs. A careful analysis of the damped modes have been carried out by tracking in time the peaks of the oscillations after Fourier analyzing in time the code results. A weakly growing tearing mode has also been observed at the radial location where $q = 3$. All the three codes demonstrate their ability to describe the MHD spectra, in quite remarkable agreement among each other; generally speaking, a very good agreement is observed while comparing the real frequencies of global modes (e.g., TAEs), while they show quite different damping, with MEGA exhibiting stronger damping than HYMAGYC and ORB5.

When considering the most unstable EP driven mode obtained by the three codes for the nominal NLED-AUG reference cases (peaked on-axis and off-axis EP density profiles), a remarkable agreement is observed among the three codes for the peaked off-axis case, obtaining all of them a TAE localized close to the magnetic axis, where the EP density profile is characterized by positive radial gradient. On the other hand, when considering the peaked on-axis case, HYMAGYC and MEGA observe, as the most unstable mode, a RSAE localized around mid-radius, whereas ORB5 observes a externally localized TAE. Looking for the dependence of the EP driven modes observed in this benchmark on the EP drive intensity, by varying consistently either the EP density or the temperature while keeping constant the radial profiles, i.e., by varying either $n_{h0}$ or $T_{h0}$, allows to reconcile the discrepancy observed for the nominal, peaked on-axis EP density profile results. Indeed, all the three codes observe, for low EP density values, a dominant externally localized TAE; this mode, as the EP density is raised, becomes, eventually, sub dominant to a stronger RSAE. The occurrence of the "cross-over" between RSAE and TAE depends strongly on the different damping experienced by the codes, which reflects in considerable variations of the net growth rates observed for this particular case (peaked on-axis EP density profile). Nevertheless, when looking carefully to the dependence of the growth rates on the EP density and temperature, all the three codes show quite similar slopes, reflecting a similar EP drive. It is to be noted that in this benchmark we are comparing the net growth rate obtained by the three codes, while, e.g., in other benchmark exercises, only the EP drive was compared [44].

Future extension of this benchmark will envisage the inclusion of finite Larmor radius (FLR) effects (here neglected), the extension to non-linear saturation regimes, the study of wave-particle power exchange to investigate in more detail wave-particle interactions and drive, together with the use of more realistic EP distribution functions (e.g., anisotropic slowing-down, etc.) and higher toroidal mode number $n$.

**Acknowledgments**

This work has been carried out within the framework of the EUROfusion Consortium and has received funding from the Euratom research and training programme 2014-2018 and 2019-2020 under grant agreement No 633053. The views and opinions expressed herein do not necessarily reflect those of the European Commission. The computing resources and the related technical support used for this work have been provided by EUROfusion and the EUROfusion High Performance Computer (Marconi-Fusion).

## References

[1] MET Enabling Research Project, `https://www.afs.enea.it/zonca/METproject/index.html`
[2] Aymar R. et al. 1997 in Proceedings of the 16th International Conference on Fusion Energy 1996, Vol. 1 (International Atomic Energy Agency, Vienna), p. 3
[3] JT-60SA Research Plan: `http://www.jt60sa.org/pdfs/JT-60SA_Res_Plan.pdf`
[4] DTT Interim Design Report, `https://www.dtt-project.enea.it/downloads/DTT_IDR_2019_WEB.pdf`
[5] Vlad G., Briguglio S., Fogaccia G. and Zonca F. Toward a new hybrid MHD gyrokinetic code: Progresses and perspectives. In *11th IAEA Technical Meeting on Energetic Particles in Magnetic Confinement Systems, Kyiv 21-23 Sept. 2009*, P-25, Vienna, Austria, 2009. International Atomic Energy Agency.
[6] Fogaccia G., Briguglio S. and Vlad G. In *40th European Physical Society Conference on Plasma Physics, Espoo, Finland, 1st - 5th July 2013*, volume 37D, page P4.151. European Physical Society, 2013.
[7] Fogaccia G., Vlad G. and Briguglio S. 2016 *Nucl. Fusion* **56** 112004
[8] Todo Y. and Sato T. 1998 *Phys. Plasmas* **5** 1321–7
[9] Todo, Y., Shinohara, K., Takechi M. and Ishikawa M. 2003 *J. Plasma Fusion Res.* **79** 1107-1108
[10] Todo Y. 2006 *Phys. Plasmas* **13** 082503
[11] Jolliet S., Bottino A., Angelino P., Hatzky R., Tran T.M., Mcmillan B.F., Sauter O., Appert K., Idomura Y. and Villard L. 2007 *Computer Physics Communications* **177** 409–425
[12] Bottino A., Vernay T., Scott B.D., Brunner S., Hatzky R., Jolliet S., McMillan B.F., Tran T.M. and Villard L. 2011 *Plasma Phys. Control. Fusion* **53** 124027
[13] Lanti E. et al. 2020 *Computer Physics Communications* **251** 107072
[14] Lauber Ph., "The NLED reference case", ASDEX Upgrade Ringberg Seminar (2016), (Ph. Lauber et al., NLED-AUG reference case, `http://www2.ipp.mpg.de/~pwl/NLED_AUG/data.html`)
[15] Ph. Lauber et al. 2018 EX1/1 Proc. 27th IAEA FEC
[16] Lütjens H., Bondeson A. and Sauter O. 1996 *Comput. Phys. Commun.* **97** 219–60
[17] Imbeaux F. et al. 2010 *Comp. Phys. Comm.* **181(6)** 987–998,
[18] Imbeaux F. et al. 2015 *Nucl. Fusion* **55** 123006
[19] Bondeson A., Vlad G. and Lütjens H. In *IAEA Technical Committee Meeting on Advances in Simulations and Modelling of Thermonuclear Plasmas, Montreal, 1992*, page 306, Vienna, Austria, 1993. International Atomic Energy Agency.
[20] Vlad G., Zonca F. and Briguglio S. 1999 *Rivista del Nuovo Cimento*, **22(7)** 1–97
[21] Bondeson A. and Fu G.Y. 1991 *Comput. Phys. Comm.* **66** 167–176
[22] Frieman E.A. and Chen L. 1982 *Phys. Fluids* **25** 502
[23] Chen L. and Zonca F. 2016 *Rev. Mod. Phys.* **88** 015008
[24] Park W., Parker S., Biglari H., Chance M., Chen L., Cheng C.Z., Hahm T.S., Lee W.W., Kulsrud R., Monticello D., Sugiyama L. and White R.B. 1992 *Phys. Fluids* B, **4** 2033
[25] Wang X., Briguglio S., Chen L., Di Troia C., Fogaccia G., Vlad G. and Zonca F. 2011 *Phys. Plasmas* **18** 052504

[26] Hazeltine R.D. and Meiss J.D. "Plasma Confinement" (Addison-Wesley, Redwood City) p.222 (1992).
[27] Tronko N., Bottino A. and Sonnendrücker E. 2016 *Physics of Plasmas* **23(8)** 082505
[28] Tronko N., Bottino A., Chandre C. and Sonnendrüecker E. 2017 *Plasma Physics and Controlled Fusion* **59(6)** 064008
[29] Mishchenko A., Bottino A., Biancalani A., Hatzky R., Hayward-Schneider T., Ohana N., Lanti E., Brunner S., Villard L., Borchardt M., Kleiber, R. and Könies A. 2019 *Computer Physics Communications* **238** 194–202
[30] Vannini F., Biancalani A., Bottino A., Hayward-Schneider T., Lauber P., Mishchenko A., Novikau I., Poli E., and ASDEX Upgrade Team 2020 *Phys. Plasmas* **27**, 042501
[31] Miyato N., Scott B.D., Strintzi D. and Tokuda S. *J. Phys. Soc. Jpn.* 2009 **78** 104501
[32] Scott B. and Smirnov J. *Physics of Plasmas* 2010 **17** 112302
[33] Krommes J.A. *Physics of Plasmas* 2013 **20** 124501
[34] Sauter O. and Medvedev S.Yu. 2013 *Computer Physics Communications* **184** 293
[35] Vlad G., Briguglio S., Fogaccia G. and Di Martino B. 2001 *Computer physics communications* **134 (1)** 58–77.
[36] Falessi M.V., Carlevaro N., Fusco V., Vlad G. and Zonca, F. 2019 *Phys. Plasmas* **26** 082502
[37] Falessi M.V., Carlevaro N., Fusco V., Giovannozzi E., Lauber Ph., Vlad G. and Zonca, F. 2020 *J. Plasma Phys.* **86** 845860501
[38] Blackman R.B. and Tukey J.W., 1958 *The measurement of power spectra* Dover Publications, New York.
[39] Press W.H., Teukolsky S.A., Vetterling W.T., Flannery B.P. 2007 *Numerical Recipes: The Art of Scientific Computing* (3rd ed.). New York: Cambridge University Press
[40] Chen L., White R.B. and Rosenbluth M.N. 1984 *Phys. Rev. Lett.* **52** 1122–1125
[41] Gorelenkov N.N. and Sharapov S.E. 1992 *Phys. Scr.* **45** 163
[42] Mett R.R. and Mahajan S.M. 1992 *Phys. Fluids B* **4** 2885
[43] Chen L. 1994 *Phys. Plasmas* **1** 1519
[44] Könies A., Briguglio S., Gorelenkov N., Fehér T., Isaev M., Lauber Ph., Mishchenko A., Spong D.A, Todo Y., Cooper W.A., Hatzky R., Kleiber R., Borchardt M., Vlad G., Biancalani A., Bottino A. and ITPA EP TG 2018 *Nucl. Fusion* **58** 126027